Modeling and optimization of the multichannel spark discharge *

Zhi-Bo Zhang (张志波)[1], Yun Wu (吴云) [1,2†], Min Jia (贾敏)[1], Hui-Min Song (宋慧敏)[1], Zheng-Zhong Sun (孙正中)[3] and Ying-Hong Li (李应红)[1]

[1] *Science and Technology on Plasma Dynamics Laboratory, Air Force Engineering University, Xi'an, 710038, People's Republic of China*
[2] *Science and Technology on Plasma Dynamics Laboratory, Xi'an Jiaotong University, Xi'an, 710049, People's Republic of China*
[3] *Department of Mechanical Engineering and Aeronautics, City University London, London, United Kingdom*

Abstract: This paper reports a novel analytic model of this multichannel spark discharge, considering the delay time in the breakdown process, the electric transforming of the discharge channel from a capacitor to a resistor induced by the air breakdown, and the varying plasma resistance in the discharge process. The good agreement between the experimental and the simulated results validated the accuracy of this model. Based on this model, the influence of the circuit parameters on the maximum discharge channel number (MDCN) is investigated. Both the input voltage amplitude and the breakdown voltage threshold of each discharge channel play a critical role. With the increase of the input voltage and the decrease of the breakdown voltage, the MCDN increases almost linearly. With the increase of the discharge capacitance, the MDCN first rises and then remains almost constant. With the increase of the circuit inductance, the MDCN increases slowly but decreases quickly when the inductance increases over a certain value. There is an optimal value of the capacitor connected to the discharge channel corresponding to the MDCN. At last, based on these results, to shorten the discharge time, a modified multichannel discharge circuit is developed and validated by the experiment. With only 6 kV input voltage, 31 channels discharge is achieved. The breakdown voltage of each electrode gap is larger than 3 kV. The modified discharge circuit is certain to be widely used in the PSJA flow control field.

Keywords: multichannel discharge circuit; circuit model; PSJA array; plasma flow control

PACS: 52.50.Dg, 52.30.-q, 50.80.Mg, 47.85.L

1 Introduction

As a promising active flow control method, the plasma flow control is an emerging research hotspot. The wide and promising prospect of this technology has been validated in many flow control fields, such as the separation control, jet boundary-layer transition control, high speed jet control, noise mitigation [1-6]. Same

* Project supported by the National Natural Science Foundation of China (51336011, 51522606, 91541120, 51611130198, 51407197 and 11472306) and Royal Society (IE150612)
† Corresponding author. E-mail: wuyun1223@126.com

as the traditional surface dielectric barrier discharge actuators (SDBD), the plasma synthetic jet actuator (PSJA) has the advantage of lack of moving part. Moreover, the PSJA can produce high-speed pulsed jet. The characteristic drives the PSJA to be applied in the high-speed flow control field successfully, such as shock-wave/boundary-layer interaction control[7,8], shock-wave manipulation, and so on [9,10].

The low efficiency of the PSJA has been validated by many experiment and simulation results [11-14]. Increasing the distance of the discharge region can improve the efficiency. But the distance is restricted by the input voltage. What's more, PSJA actuator is different from the SDBD actuator[15], which can be used to meter scale. The orifice of the PSJA is only onin the order of millimeter[16,17], which is far less than the region of the flow field needed to be affected. To solve these two problems, the PSJA array is necessary in the practical application. Based on a pulsed DC discharge circuit, the team of Clemens used a PSJA array to control of the shock/boundary-layer interaction[7,10]. The PSJA array consisted of only 3 PSJAs, which was far from the number needed in the practical application. And owing to the large current-limiting resistor in the discharge circuit, most of the energy is wasted by the circuit resistor. Therefore, this circuit is not efficient to drive the PSJA array. However, different from the barrier discharge[18,19], the resistance characteristic of the arc discharge channel is negative. As a result, it is difficult to drive the PSJA in serials by a power supply. As a result, several power supplies are needed to drive the actuator array, which is apparently not feasible in practice. Tie et al. proposed a six channel spark discharge method [20]. However, the necessary condition of very high trigger voltage (40 kV) and short rise time (25 ns) increases the technical requirements for the power supply.

To solve this problem, a special multichannel discharge circuit is presented developed by us, which can drive the multichannel discharge using only one supply circuit[21]. And no extra resistor is necessary in this circuit. However, the electric characteristics of this circuit are not clear currently. The relationship between the circuit parameters and the maximum discharge channel number (MDCN) has not been uncovered. That how to choose the circuit parameters lacks of guiding theory.

In this paper, an electric model on this multichannel discharge circuit is put forward, which is validated by experimental data. Using this model, the influence of the circuit parameters on the MDCN is investigated. Based on the influence rules, an optimization of the multichannel discharge circuit is obtained and validated by the experiment.

2 The model of the multichannel discharge circuit

2.1 The multichannel discharge circuit

To achieve the multichannel discharge, a principle circuit is designed, which is

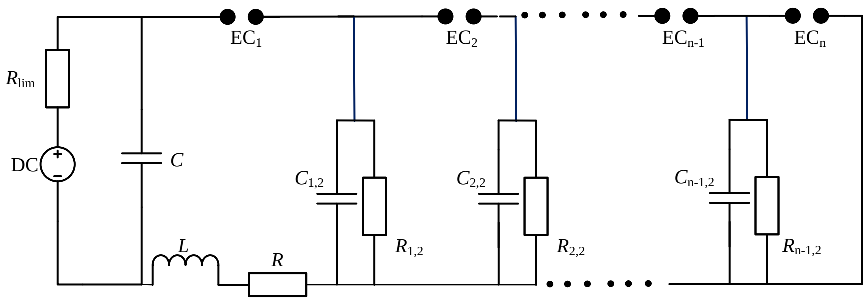

shown in

Fig. 1. A high voltage DC power system is adopted as the power supply. The discharge frequency can be adjusted by changing the current limiting resistor R_{lim}. The inductance L represents the wire inductance. The inductance R represents the wire resistance and the equivalent series resistance of the capacitor C. The discharge energy is controlled by the capacitor C and the breakdown voltage of the first electrode couple (EC) EC_1. The relay capacitor, $C_{1,2}$, $C_{2,2}$,…,$C_{n-1,2}$, and the resistor, $R_{1,2}$, $R_{2,2}$,…, $R_{n-1,2}$ are used to relay the high voltage and ensure the multichannel discharge.

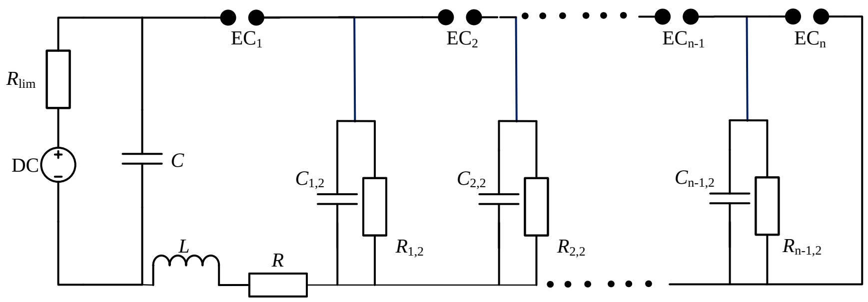

Fig. 1. The multichannel discharge circuit diagram

2.2 Model establishment

2.2.1 Basic assumptions

To establish this simulation model, some assumptions must be made.

A) The electrode couple is seen as a capacitor before breakdown and a variable resistor after breakdown. The variable resistance is calculated based on an improved mayr-type arc model developed by Pieter H. Schavemaker[22].

B) The breakdown voltage amplitude of the electrode couple is not fixed. The distribution satisfies the normal assumption.

C) The breakdown delay time is not fixed. The distribution satisfies the normal assumption. The mean breakdown delay time is calculated using an empirical formula[23].

D) When the breakdown of electrode couple EC_i does not happen, the current in the next electrode couple is ignored.

2.2.2 The main submodels

To simulate the multichannel discharge process, there are three main submodels. The first submodel is used to decide whether or not the breakdown of one electrode couple happens. When the breakdown happens, the electrode couple transforms from a capacitor to a variable resistor. The second submodel is used to calculate the voltage-current characteristic of the variable resistor. The last submodel is used to decide whether or not the spark channel between the electrode couple terminates.

Breakdown process is a complex process. The breakdown of one electrode couple is a random process. Even in a same condition, it is not definite that whether or not the breakdown of one electrode couple happens. In this submodel, the decision criterions are defined as following:

A) The voltage amplitude across the electrode couple must increase to a threshold value. The distribution of the threshold values in different times meets the normal assumption. The mean value is calculated by equation (1). p represents the pressure, which is in bars; d is the distance between the electrode couple, which is in centimeters. The standard deviation of the normal distribution stands for the disturbance level.

$$U_{\mathrm{breakdown}} = 24.36pd + 6.72\sqrt{pd} \quad (\mathrm{kV}) \tag{1}$$

B) The above condition must remain a certain time, which is called the breakdown delay time. The distribution of the breakdown delay time values in different times meets the normal assumption. The mean value is calculated by an empirical formula, as equation (2). ρ is the air density in g/cm^3. E is the average electric field in kV/cm.

$$T_{\mathrm{delay}} = 97800\frac{\rho^{2.44}}{E^{3.44}} \quad (\mathrm{s}) \tag{2}$$

The voltage-current characteristic of the variable resistor is calculated based on an improved mayr-type arc model developed by Pieter H. Schavemaker. The arc model is described by the following equation. g is the arc conductance; U is the arc voltage; I is the arc current; τ is time constant; P_0 is the cooling power; P_1 is the cooling power affected by the heating power; e_0 is the constant arc voltage in the high current area.

$$\frac{dg}{dt} = \frac{1}{\tau}\left(\frac{UI}{\max(P_0 + P_1UI, e_0|I|)} - 1\right)g \tag{3}$$

After breakdown, the arc conductance changes with the arc current and arc voltage. In this simulation model, when the arc conductance decreases to a threshold value, the discharge channel between the electrode couple is supposed to disappear.

2.2.3 The differential equations of the multichannel discharge circuit

Based on the above assumptions, after the breakdown of the electrode couple EC$_i$(i<n-1), the discharge circuit diagram can been simplified, as shown in Fig. 2.

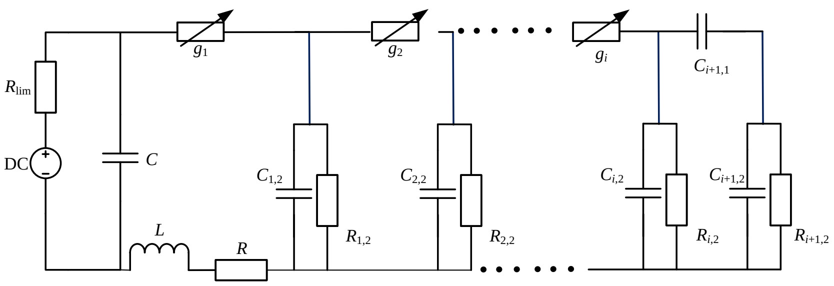

Fig. 2. The simplified circuit diagram after the breakdown of ECi

The differential equations of the above circuit are shown in equations (4). In this equation, $U_{x,2}$ means the voltage across the capacitor $C_{x,2}$. For example, $U_{1,2}$ is the voltage across the capacitor $C_{1,2}$. The I_x means the current flowing through the electrode couple EC_x. The g_x represents the arc conductance of the electrode couple EC_x. The C_1 stands for the equivalent capacitance of the electrode couple, which is supposed as 1 pF. The C_2 means the capacitance of the capacitor $C_{x,2}$. The R_2 is the resistance of the resistor $R_{x,2}$. Owing to the same value, for convenient calculation, these capacitors and resistors are not distinguished in these equations.

$$\begin{cases}
\frac{dU}{dt} = -\frac{1}{C_0}(\frac{U_0 - U}{R_{\lim}} - I_1) \\
\frac{dI_1}{dt} = \frac{1}{L}\left(U - I_1 / g_1 - U_{1,2} - RI_1\right) \\
\frac{dg_1}{dt} = \frac{1}{\tau}\left(\frac{I_1^2 / g_1}{\max\left(P_0 + P_1 I_1^2 / g_1, e_0 \left|I_1\right|\right)} - 1\right) g_1 \\
\frac{dU_{1,2}}{dt} = \frac{1}{C_2}\left(I_1 - \frac{U_{1,2}}{R_2} - \left(U_{1,2} - U_{2,2}\right) g_2\right) \\
\frac{dg_2}{dt} = \frac{1}{\tau}\left(\frac{\left(U_{1,2} - U_{2,2}\right)^2 g_2}{\max\left(P_0 + P_1\left(U_{1,2} - U_{2,2}\right)^2 g_2, e_0 \left|\left(U_{1,2} - U_{2,2}\right) g_2\right|\right)} - 1\right) g_2 \\
\cdots \\
\frac{dU_{k,2}}{dt} = \frac{1}{C_2}\left(\left(U_{k-1,2} - U_{k,2}\right) g_k - \frac{U_{k,2}}{R_2} - \left(U_{k,2} - U_{k+1,2}\right) g_{k+1}\right) \\
\frac{dg_{k+1}}{dt} = \frac{1}{\tau}\left(\frac{\left(U_{k,2} - U_{k+1,2}\right)^2 g_{k+1}}{\max\left(P_0 + P_1\left(U_{k,2} - U_{k+1,2}\right)^2 g_{k+1}, e_0 \left|\left(U_{k,2} - U_{k+1,2}\right) g_{k+1}\right|\right)} - 1\right) g_{k+1} \\
\cdots \\
\frac{dU_{i,2}}{dt} = \frac{1}{C_2^2 + 2C_1C_2}\left(\left(C_1 + C_2\right)\left(U_{i-1,2} - U_{i,2}\right) g_i - \frac{C_1 + C_2}{R_2} U_{i,2} - \frac{C_1}{R_2} U_{i+1,2}\right) \\
\frac{dU_{i+1,2}}{dt} = \frac{1}{C_2^2 + 2C_1C_2}\left(C_1\left(U_{i-1,2} - U_{i,2}\right) g_i - \frac{C_1}{R_2} U_{i,2} - \frac{C_1 + C_2}{R_2} U_{i+1,2}\right)
\end{cases} \quad (4)$$

When the breakdown of the electrode couple EC_{n-1} happens, the circuit diagram can't be described as Fig. 2. The corresponding diagram is shown in Fig. 3. The corresponding differential equations change as well, which are expressed in equation (5).

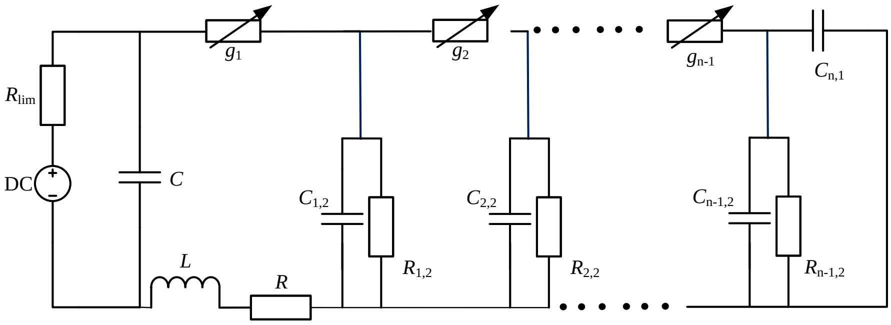

Fig. 3. The simplified circuit diagram after the breakdown of ECn-1

$$
\begin{cases}
\dfrac{dU}{dt}=-\dfrac{1}{C_0}\left(\dfrac{U_0-U}{R_{\lim}}-I_1\right)\\
\dfrac{dI_1}{dt}=\dfrac{1}{L}\left(U-I_1/g_1-U_{1,2}-RI_1\right)\\
\dfrac{dg_1}{dt}=\dfrac{1}{\tau}\left(\dfrac{I_1^2/g_1}{\max\left(P_0+P_1I_1^2/g_1,e_0\left|I_1\right|\right)}-1\right)g_1\\
\dfrac{dU_{1,2}}{dt}=\dfrac{1}{C_2}\left(I_1-\dfrac{U_{1,2}}{R_2}-\left(U_{1,2}-U_{2,2}\right)g_2\right)\\
\dfrac{dg_2}{dt}=\dfrac{1}{\tau}\left(\dfrac{\left(U_{1,2}-U_{2,2}\right)^2g_2}{\max\left(P_0+P_1\left(U_{1,2}-U_{2,2}\right)^2g_2,e_0\left|\left(U_{1,2}-U_{2,2}\right)g_2\right|\right)}-1\right)g_2\\
\dots\\
\dfrac{dU_{k,2}}{dt}=\dfrac{1}{C_2}\left(\left(U_{k-1,2}-U_{k,2}\right)g_k-\dfrac{U_{k,2}}{R_2}-\left(U_{k,2}-U_{k+1,2}\right)g_{k+1}\right)\\
\dfrac{dg_{k+1}}{dt}=\dfrac{1}{\tau}\left(\dfrac{\left(U_{k,2}-U_{k+1,2}\right)^2g_{k+1}}{\max\left(P_0+P_1\left(U_{k,2}-U_{k+1,2}\right)^2g_{k+1},e_0\left|\left(U_{k,2}-U_{k+1,2}\right)g_{k+1}\right|\right)}-1\right)g_{k+1}\\
\dots\\
\dfrac{dU_{n-1,2}}{dt}=\dfrac{1}{C_1+C_2}\left(\left(U_{n-2,2}-U_{n-1,2}\right)g_{n-1}-\dfrac{U_{n-1,2}}{R_2}\right)
\end{cases}
\tag{5}
$$

When the breakdown of the electrode couple EC_n happens, a complete discharge circuit is built, which is shown in

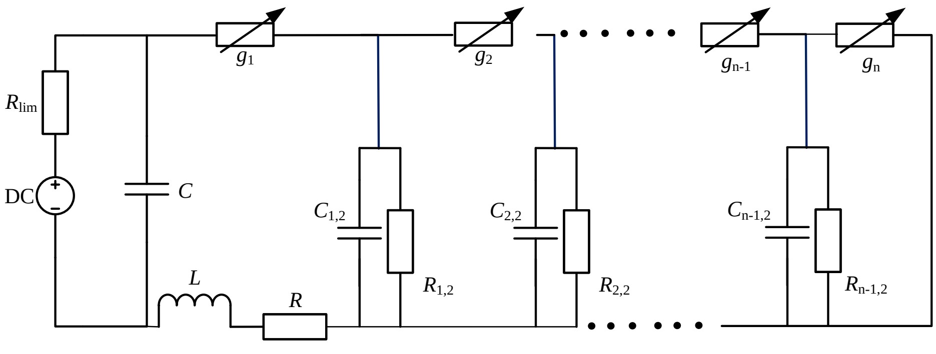

Fig. 4. The corresponding differential equations are expressed in equation (6).

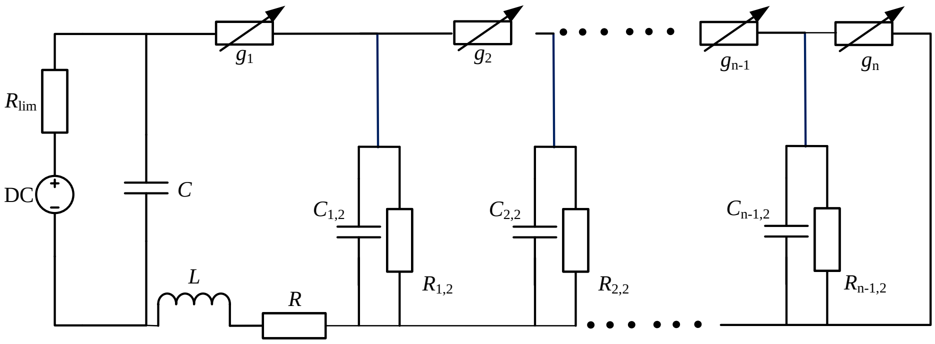

Fig. 4. The simplified circuit diagram after the breakdown of ECn

$$\begin{cases} \dfrac{dU}{dt} = -\dfrac{1}{C_0}\left(\dfrac{U_0 - U}{R_{\lim}} - I_1\right) \\ \dfrac{dI_1}{dt} = \dfrac{1}{L}\left(U - I_1 / g_1 - U_{1,2} - RI_1\right) \\ \dfrac{dg_1}{dt} = \dfrac{1}{\tau}\left(\dfrac{I_1^2 / g_1}{\max\left(P_0 + P_1 I_1^2 / g_1, e_0 \left|I_1\right|\right)} - 1\right) g_1 \\ \dfrac{dU_{1,2}}{dt} = \dfrac{1}{C_2}\left(I_1 - \dfrac{U_{1,2}}{R_2} - \left(U_{1,2} - U_{2,2}\right) g_2\right) \\ \dfrac{dg_2}{dt} = \dfrac{1}{\tau}\left(\dfrac{\left(U_{1,2} - U_{2,2}\right)^2 g_2}{\max\left(P_0 + P_1\left(U_{1,2} - U_{2,2}\right)^2 g_2, e_0 \left|\left(U_{1,2} - U_{2,2}\right) g_2\right|\right)} - 1\right) g_2 \\ \cdots \\ \dfrac{dU_{k,2}}{dt} = \dfrac{1}{C_2}\left(\left(U_{k-1,2} - U_{k,2}\right) g_k - \dfrac{U_{k,2}}{R_2} - \left(U_{k,2} - U_{k+1,2}\right) g_{k+1}\right) \\ \dfrac{dg_{k+1}}{dt} = \dfrac{1}{\tau}\left(\dfrac{\left(U_{k,2} - U_{k+1,2}\right)^2 g_{k+1}}{\max\left(P_0 + P_1\left(U_{k,2} - U_{k+1,2}\right)^2 g_{k+1}, e_0 \left|\left(U_{k,2} - U_{k+1,2}\right) g_{k+1}\right|\right)} - 1\right) g_{k+1} \\ \cdots \\ \dfrac{dU_{n-1,2}}{dt} = \dfrac{1}{C_2}\left(\left(U_{n-2,2} - U_{n-1,2}\right) g_{n-1} - \dfrac{U_{n-1,2}}{R_2} - U_{n-1,2} g_n\right) \\ \dfrac{dg_n}{dt} = \dfrac{1}{\tau}\left(\dfrac{U_{n-1,2}^2 g_n}{\max\left(P_0 + P_1 U_{n-1,2}^2 g_n, e_0 \left|U_{n-1,2} g_n\right|\right)} - 1\right) g_n \end{cases} \tag{6}$$

2.2.4 The simulation procedure

Based on the above submodels and differential equations, the multichannel discharge process can be simulated. The simulation flow chart is shown in Fig. 5. In this figure, A represents the state parameters of the circuit, which are calculated by solving the above differential equations. The simulation begins with the breakdown of the first electrode couple. If any of the arc channel terminates, the simulation stops and outputs the calculation results. If breakdown happens in all electrode couples, it means the multichannel discharge circuit works properly. Otherwise, it means the multichannel discharge circuit fails to achieve multichannel discharge.

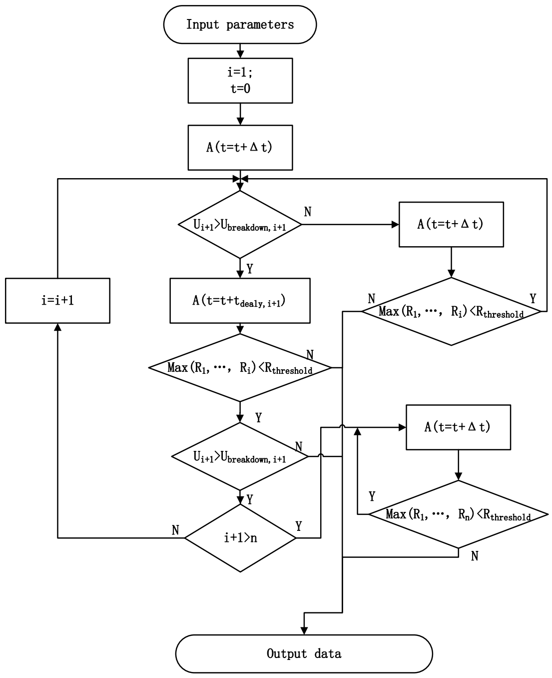

Fig. 5. The simulation flow chart

2.3 Model validation

To validate the simulation model, an experiment system is built, as shown in Fig. 6. To improve the accuracy of the experimental data, the discharge electrodes are made of two stainless steel spheres. The diameter of the sphere is up to 25 mm, larger than the electrode couple distance. The two steel spheres are fixed on two micro positioning systems (sensitivity 1 μm), respectively. The voltage and the current are measured by a high-voltage probe (Tektronix, P6015) and a current probe (Pearson, 6600), respectively. An oscilloscope (Tektronix, DPO4014) is used to display and record the data. In this experiment, the capacitor C is 1 nF, the inductance is 1.63 μH, the total value of wire resistance and equivalent series capacitor resistance is 1.89 Ω. The values of capacitance and resistance are obtained by an impedance analyzer (Agilent 4285A).

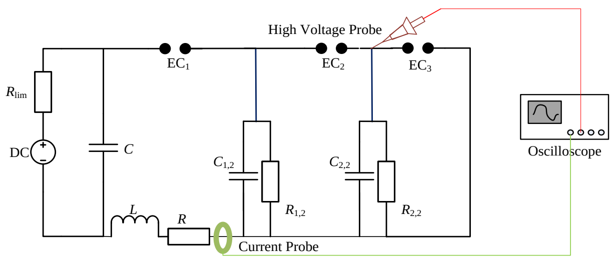

Fig. 6. Experiment system

When the distance of EC_2 and EC_3 are set 0 mm, this discharge circuit is the traditional one channel discharge circuit. Based on the measured current of the one channel discharge circuit, these parameters of Schavemaker arc model are determined from the least squares fit: τ=2.28e-08 s, P_0=219 W, P_1=0.39 and e_0=56.41 V. As shown in Fig. 7, the simulation result shows a good agreement with the experiment result.

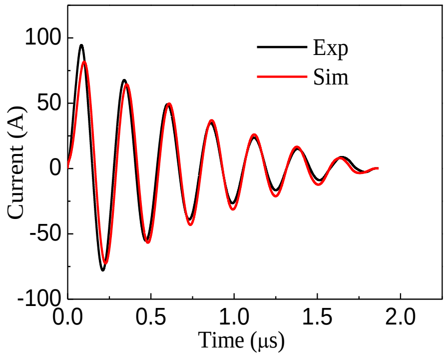

Fig. 7. The measured and simulated current waveforms

Based on these parameters, three channel discharge circuit is simulated. The measured and simulated results are shown in Fig. 8. The simulated current waveform shows a good agreement with the experimental current waveform. After the breakdown of the first electrode couple, EC_1, the gap transforms from a capacitor to a resistor, and the capacitor $C_{1,2}$ begins to be charged. Then the current in the circuit increases. At about 132 ns, the breakdown of the last electrode couple happens, all arc channels connected with each other by wire directly. At this time, the current increases greatly. The simulated voltage waveform is similar with the experimental voltage waveform, except the great oscillation after breakdown. At about 61 ns, the breakdown of the second electrode couple happens, the electric characteristic of the electrode couple EC_2 began to change from a capacitor to a resistor. Then the voltage across the capacitor $C_{2,2}$ increases. In totally, the simulation model can catch the characteristics of the multichannel discharge circuit.

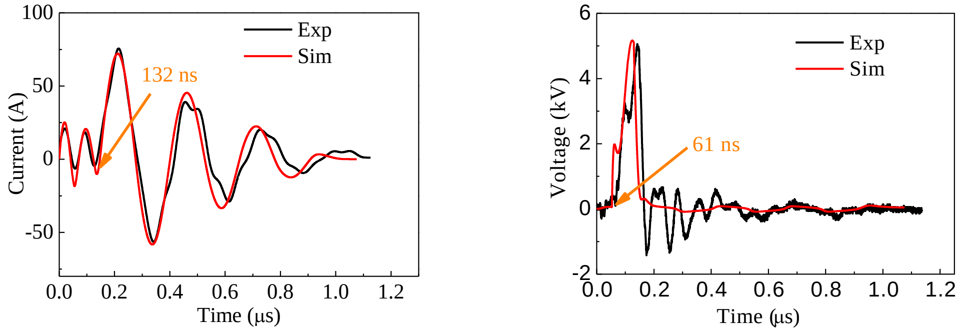

Fig. 8. (color online) The measured and simulated results: (a) Current waveform (b) Voltage waveform

3 Results and discussion

This novel multichannel discharge circuit can multiply the discharge channel. Based on this method, the region affected by the plasma actuators can be enlarged. To further understand this circuit, the characteristics of this circuit must be investigated.

3.1 The working mechanism of the multichannel discharge circuit

Owing to negative current-voltage (I-V) character of the spark discharge, as previously reported[24], the array of discharge can be only generated by using a distributed resistive ballast previously, where each spark discharge is individual ballast. However, in this special circuit, array of discharge is generated without resistance ballast. Based on this model, the working mechanism of this circuit can be revealed in detial.

In a 5 channels discharge circuit, the voltage across C, $C_{1,2}$, $C_{2,2}$, $C_{3,2}$ and $C_{4,2}$ is plotted in Fig. 9. To show the impedance change induced by breakdown, the voltage across EC_2 (U_{EC2}) and discharge current are plotted in Fig. 10. After the breakdown of the first electrode couple, the voltage across the capacitor $C_{1,2}$ increases quickly. However, with the increase of $U\text{c}_{1,2}$, the voltage across the capacitor $C_{2,2}$ keeps almost 0 V until the breakdown of EC_2. In other words, the U_{EC2} is the same as $U\text{c}_{1,2}$ until the breakdown of EC_2 happens. And the impedance of relay capacitor $C_{2,2}$ can be ignored before the breakdown of EC_2. At about 66 ns, the breakdown of EC_2 induces that the electrode couple EC_2 changes from an equivalent capacitor to an equivalent resistor. Meanwhile, the voltage across the capacitor $C_{2,2}$ increases quickly, while the voltage across the EC_2 decreases. At about 144 ns, the U_{EC2} has decreases to only 58.5 V. As a reuslt, $U\text{c}_{2,2}$ has increased to a high value, which can be used to ignite the third electrode couple (EC_3). As a reuslt, the remained electrode couples are broken down in sequence, which can be revealed by the variation of the voltage across the capacitor $C_{3,2}$ and $C_{4,2}$. So the total discharge process can be separated into two processes: trigger discharge and spark discharge. The trigger discharge process starts from the breakdown of the first electrode gap and ends with the breakdown of the last electrode gap. The remaining rest of the process is the spark discharge.

It is known that, to ingite the air between the electrode couple, the high voltage is necessary. Before the breakdown of each electrode couple, the electrode couple, which can be seen as a small capacity capacitor, is connected with a large relay capacitor in serials. Therefore, when the power supply outputs the pulsed voltage, the impedance of relay capacitor can be ignored. The voltage across the electrode couple would increase until the breakdown. As the negative current-voltage (I-V) character of the spark discharge, the voltage drop of an ignited electrode couple is so small that the discharge channel can be seen as wire. As a result, the voltage across the next electrode couple would increase until the breakdown. Taking advantage of the negative current-voltage (I-V) character of the spark discharge and the impedance change induced by the breakdown, this circuit can generate multichannel discharge without distributed resistive ballast.

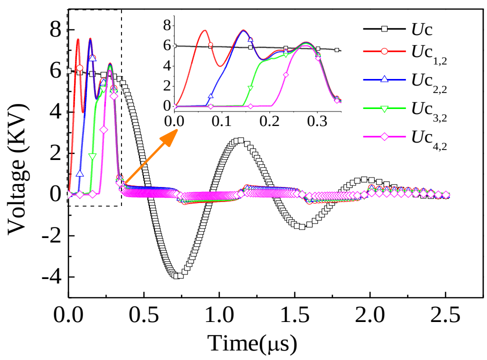

Fig. 9. (color online) The voltage across different capacitor

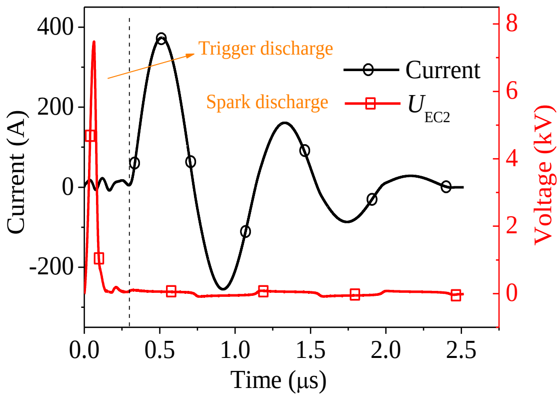

Fig. 10. (color online) The discharge current and the voltage across the second electrode couple

To ensure this circuit work properly, two aspects must be paid attention to. One is that the breakdown voltage of the electrode couple EC_2, EC_3,…, EC_n should be less than that of the electrode couple EC_1. Another is that the discharge channel must remain alive until breakdown happens in all electrode gaps. These two aspects are affected by the circuit parameters, which is investigated in the following.

3.2 The influence of circuit parameters

The main parameters of this circuit which affects the maximum discharge channel number are shown in Table 1. As described above, the breakdown voltage and the breakdown delay time are not fixed. When the parameters of the circuit keep unchanged, the maximum number of the discharge channels varies. Therefore, in this paper, in a given condition, the simulation is done for 100 times. If the multichannel discharge circuit works properly in above 90 times, the number of the electrode couple increases one. Otherwise, the number of the electrode couple is the maximum number of discharge channel in this given condition.

Table 1. The main parameters of the multichannel discharge circuit

Parameter	Meaning
U_1	The mean voltage across the capacitor C before breakdown, which is determined by the distance of the first electrode couple
U_2	The mean breakdown voltage of the electrode couple, EC_2, EC_3,…,EC_n
C_0	The capacitance of the main discharge capacitor C
L	The inductance of the circuit
C_2	The capacitance of the capacitor $C_{1,2}$, $C_{2,2}$, …,$C_{n-1,2}$

3.2.1 The influence of U_1

Except the U_1, the value of other parameters is set as following: U_2=4000 V, C_0=10 nF, C_2=0.2 nF, R_2=1 MΩ, L=1.65 μH. The MDCN versus U_1 is shown in Fig. 11. When the voltage across capacitor C (U_1) increases, the MDCN almost increases linearly.

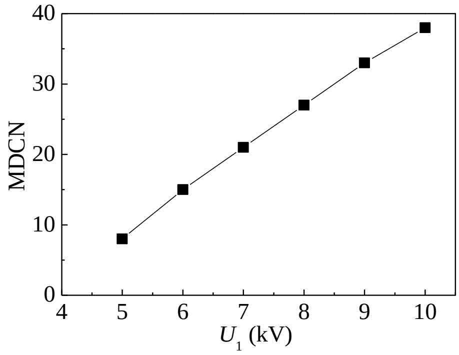

Fig. 11. The maximum of discharge channels versus U_1

This phenomenon is easy to explain. Equation (2) has indicated that high electric field strength leads to a short breakdown delay time. So the time to form a complete discharge channel from the first electrode couple EC_1 to the last electrode couple EC_n decreases with the increase of the voltage U_1. The short time benefits that the formed discharge channel keeps live. What's more, with the increase of voltage U_1, the current in the trigger discharge process increases. As a result, more energy is deposited in the discharge channel, which can prevent the discharge channel to terminate. The time to form 5 discharge channels for different voltage U_1 is plotted in Fig. 12. The current waveforms in the trigger discharge process for different voltage U_1 is plotted in Fig. 13. These two figures can validate the claim.

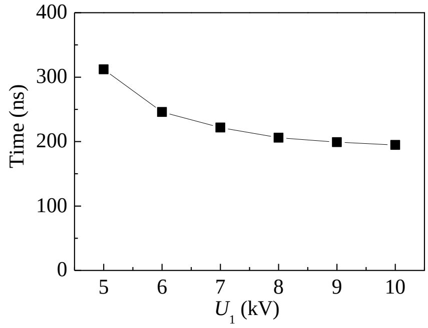

Fig. 12. The time to form 5 discharge channels versus U_1

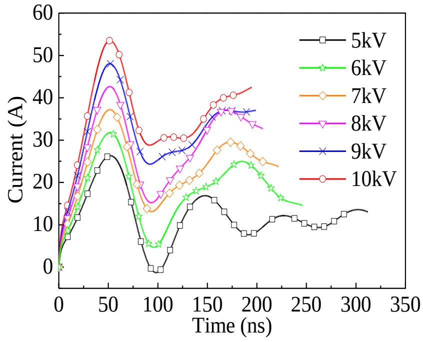

Fig. 13. (color online) The current waveforms versus U_1

3.2.2 The influence of U_2

Except the U_2, the value of other parameters is set as following: U_1=10000 V, C_0=10 nF, C_2=0.2 nF, R_2=1 MΩ, L=1.65 μH. The MDCN versus U_2 is shown in Fig.

14. Obviously, with the increase of voltage U_2, the MDCN almost decreases linearly.

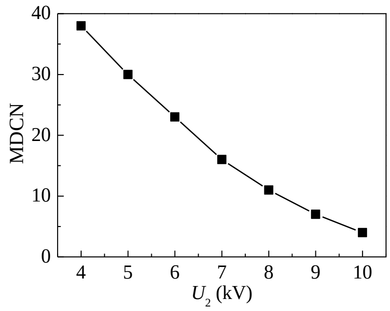

Fig. 14. The maximum discharge channel number versus U_2

In generally, the increase of U_2 presents the increase of the distance of electrode couple. As the voltage U_0 is fixed, with the increase of U_2, the overvoltage decrease. As a result, the electric field intensity within the air between the electrode couple decreases, leading the increase of breakdown delay time. Meanwhile, the current in the trigger discharge process decreases. This change does harm to the increase of discharge channel number.

3.2.3 The influence of C_0

Except the C_0, the value of other parameters is set as following: U_1=6000 V, U_2=4000 V, C_2=0.2 nF, R_2=1 MΩ, L=1.65 μH. The maximum of discharge channel number versus C_0 is shown in Fig. 15. Obviously, with the increase of voltage C_0, the maximum of discharge channel number increases. However, over a certain value of the capacitance C_0, its effect becomes more and more weak. Therefore, to increase the MDCN, it is better to increase the voltage U_0 rather than the capacitance C_0.

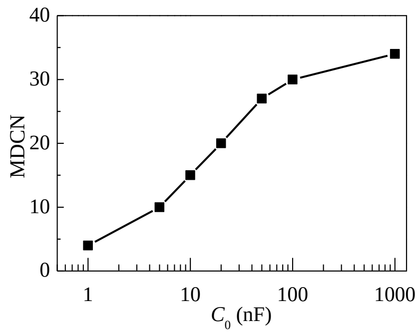

Fig. 15. The maximum of discharge channels versus C_0

3.2.4 The influence of C_2

Except the C_2, the value of other parameters is set as following: U_1=6000 V, U_2=4000 V, C_0=10 nF, R_2=1 MΩ, L=1.65 μH. The MDCN versus C_2 is shown in Fig. 16. This figure indicates that there is an optimized value of the capacitance C_2, about 100 pF. When the capacitance C_2 is larger or smaller than this value, the MDCN decreases.

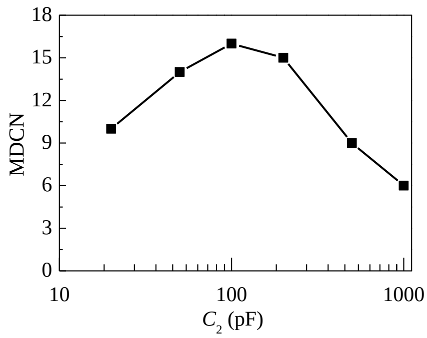

Fig. 16. The maximum of discharge channels versus C_2

The reason for this phenomenon is as following. With the decrease of the capacitance C_2, the current in the trigger discharge process decreases. Less energy is deposited in the discharge channel. As a result, the formed discharge channel is easy to terminate. The current waveforms in the trigger discharge process for different capacitance C_2 is plotted in Fig. 17, which can show the variation of current with the capacitance C_2. However, with the increase of the relay capacitanceC_2, more energy is needed to charge these relay capacitors to the same voltage. As the energy stored in the capacitor C is fixed, the discharge channel number decreases.

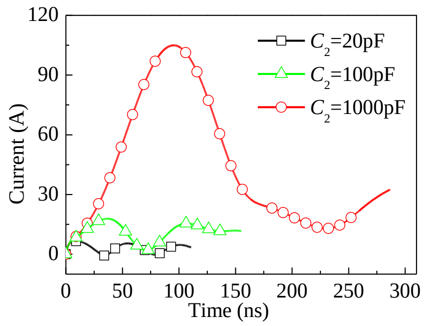

Fig. 17. (color online) The current waveforms versus C_2

3.2.5 The influence of *L*

Except the *L*, the value of other parameters is set as following: U_1=6000 V, U_2=4000V, C_0=10 nF, C_2=100 pF, R_2=1 MΩ. The maximum of discharge channel number versus *L* is shown in Fig. 18. There are three stages in this curve. In the first stage, the inductance is less than 16.5 μH, and the maximum discharge channel number ranges from 16 to 18. With the inductance increases to a large value, the maximum discharge channel number increase to a higher stage, ranging from 22 to 25. But when the inductance increases too large, the discharge channel number decreases to only one.

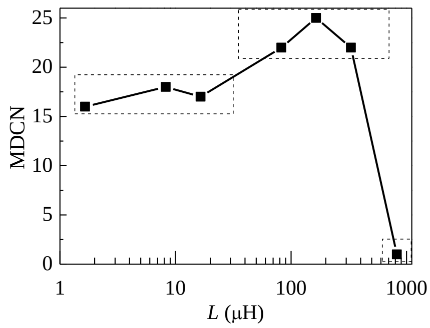

Fig. 18. The maximum of discharge channels versus L

3.3 The optimization of the discharge circuit

Based on the self-made mathematical model, the influence of the multichannel discharge circuit parameters is investigated. These parameters can be decided into two categories. One can be not randomly changed to increase the discharge channel number. The voltage U_1 is limited by the power supply system. The capacitor C_0 is limited by the discharge frequency. The voltage U_2 is limited by the plasma actuator. Another can be changed randomly, such as the capacitors $C_{x,2}$, the inductance L. However, with the increase of the inductance, the discharge current decreases and the discharge time increases. This goes against the improvement of the energy efficiency. In order to increase the discharge channel number without decreasing the energy efficiency, the discharge circuit must be modified. The modified circuit diagram is shown in Fig. 19. In this circuit, the inductance L_1 only plays role in the trigger discharge process. When breakdown happens in all electrode couple, the impedance of the discharge channel decreases quickly. As a result, the inductance L_1 doesn't work.

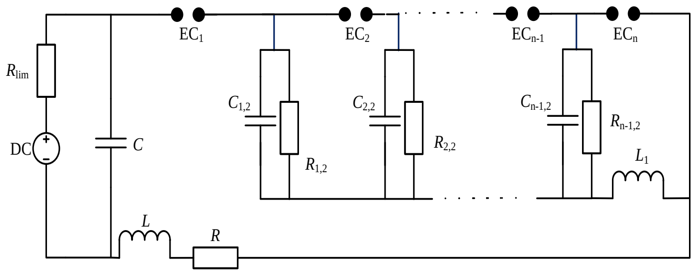

Fig. 19. The modified multichannel discharge circuit

To validate this optimized circuit diagram, based on this optimized parameters, a 31-channel discharge experiment is designed. The discharge image is shown in Fig. 20, which is captured with a Nikon D7000 camera, f-stop f/5.3, shutter speed 1/320 sec, ISO 200. The first electrode couple is made of two hemispheres, and the corresponding breakdown voltage is about 6 kV. The remained electrode couples are made of tungsten needles with 2 mm distance. Due to the tip effect, the corresponding breakdown voltage ranges from 3 to 4 kV. The discharge current and voltage waveforms are shown in Fig. 22. The voltage across the discharge capacitor C, determined by the first electrode couple, is only 6 kV. To form a completed discharge channel, the time of the trigger discharge process is as long as 6.5 μs. Owing to the increase of the plasma resistance, the spark discharge process is shortened to 0.77 μs. Based on this waveform, the plasma resistance is estimated to be 35.87 Ω.

Fig. 20. (color online) The discharge images of 31 channels

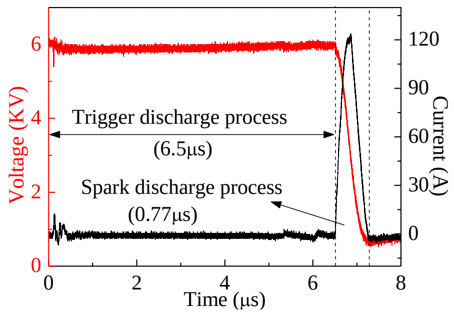

Fig. 21. (color online)The discharge voltage and current waveform with 31 discharge channels

34 Conclusions

To deepen the understanding of the electrical characteristics and optimize the multichannel discharge circuit, an electric model on a multichannel discharge circuit is developed in this paper. The good agreement between the experiment and the simulation based on this model has shown the accuracy.

Results shown there are two stages in the working process of this multichannel discharge circuit. The first stage is the trigger discharge process. By voltage relay, the voltage across the electrode couples increases to its corresponding breakdown voltage in sequence. The second stage is the spark discharge process. When breakdown happens in all electrode gaps, the discharge current increases quickly.

Based on this model, the influence of the circuit parameters on the MDCN is investigated in detail. Both the input voltage amplitude and the breakdown voltage threshold of each discharge channel play a critical role. With the increase of the input voltage and the decrease of the breakdown voltage, the MCDN increases almost linearly. With the increase of the discharge capacitance, the MDCN first rises and then remains almost constant. With the increase of the circuit inductance, the MDCN increases slowly but decreases quickly when the inductance increases over a certain value. There is an optimal value of the capacitor connected to the discharge channel corresponding to the MDCN.

Based on these influence rules, to shorten the discharge time, a modified multichannel discharge circuit is developed and validated by the experiment. With only 6 kV input voltage, 31-channel discharge is achieved. The breakdown voltage of each electrode gap is larger than 3 kV. Owing to the increase of the plasma resistance, the capacitor deposits its energy in a short time, about 770 ns.

REFERENCES

1. Corke T C, Enloe C L and Wilkinson S P 2010 Annu. Rev. Fluid Mech. 42 505-529
2. Cattafesta III L N and Sheplak M 2011 Annu. Rev. Fluid Mech. 43 247-272
3. Bletzinger P, Ganguly B N, Wie D V and Garscadden A 2005 J. Phys. D: Appl. Phys. 38 R33–R57
4. Webb N, Clifford C and Samimy M. 2013 Exp. Fluids 54 1545
5. Hahn C, Kearney-Fischer M and Samimy M 2011 Exp. Fluids 51 1591-1603
6. Samimy M, Kim J H, Kastner J, Adamovich I and Utkin Y 2007 AIAA J. 45 890-901
7. Narayanaswamy V, Raja L L and Clemens N T 2012 Phys. Fluids 24 076101
8. Greene B R, Clemens N T, Magari P and Micka D 2013 Shock Waves 25 495-505
9. Narayanaswamy V, Raja L L and Clemens N T 2010 AIAA J. 48 297-305
10. Emerick T, Ali M Y, Foster C, Alvi F S and Popkin S 2014 Exp. Fluids 55 1858
11. Golbabaei-Asl M, Knight D and Wilkinson S 2015 AIAA J. 53 501-504
12. Popkin S H, Cybyk B Z, Foster C H and Alvi F S 2016 AIAA J. 54 1831-1845
13. Zong H, Wu Y, Song H and Jia M 2016 AIAA J. 54 3409-3420
14. Zong H, Wu Y, Li Y, Song H, Zhang Z and Jia M 2015 Physics of Fluids 27 027105
15. Wu Y, Li J, Jia M, Liang H and Song H 2012 Chin. Phys. B 21 045202
16. Wang L, Luo Z, Xia Z and Liu B 2013 Acta Phys. Sin. 62 125207
17. Wang L, Xia Z, Luo Z, Zhou Y and Zhang Y 2014 Acta Phys. Sin. 63 194702
18. Zhang C, Wang Y, Zhou Y, Xie Q, Wang R, Yan P and Shao T 2016 IEEE T. Plasma SCI. 44 2772-2778
19. Shao T, Jiang H, Zhang C, Yan P, Lomaev M I and Tarasenko V F 2013. EPL-EUROPHYS LETT. 101 45002.
20. Tie W, Liu X, Liu S and Zhang Q 2015 IEEE T. Plasma SCI. 43 937–943
21. Zhang Z, Wu Y, Jia M, Song H, Sun Z, Zong H and Li Y 2017 SENSOR ACTUAT. A-PHYS. 253 112-117
22. Schavemaker P H and Van der Slui L 2000 IEEE T. Power Deliver 15 580-584
23. Martin T H 1989. Sandia National Labs. Albuquerque, NM (USA) 73-79
24. Hippler R, Kersten H and Schmidt M 2008 Low temperature plasma:fundamentals, technologies and techniques Vol 2, 2nd edn.(Wiler-VCH) p.465